Available online at www.sciencedirect.com
ScienceDirect
International Journal of Heat and Mass Transfer 51 (2008) 2190–2198
International Journal of HEAT and MASS TRANSFER
www.elsevier.com/locate/ijhmt

Lean combustibility limit of methane in reciprocal flow filtration combustion reactor

K.V. Dobrego [a,*], N.N. Gnesdilov [a], S.H. Lee [b], H.K. Choi [b]

[a] Luikov Heat and Mass Transfer Institute, Belarus Academy of Sciences, 15 P. Brovka Street, Minsk 220072, Belarus
[b] Korean Institute of Energy Research (KIER), 71-2 Jang-dong, Yuseong-gu, Daejeon 305-343, South Korea

Received 12 October 2007
Available online 8 January 2008

Abstract

Analytical and numerical investigation of methane–air lean combustibility limit (LCL) in reciprocal flow filtration combustion reactor was performed. Practically important parameters (heat loss coefficient, reactor length, pressure, particles size, porosity) were varied and corresponding sets of LCL curves were built. Existence of extremum at LCL – gas flow rate function is found. Numerical study shows that the porous media particle size is the most important factor for LCL control. Smaller particles provide lower LCL and reduce steepness of the growing branch of the LCL-gas flow rate function. For the particles smaller than 2 mm the corresponding LCL line goes down monotonously. High pressure in the system provides better LCL, which may be used for stabilization of the reactors operating at near LCL regimes.

Keywords: Filtration combustion; Lean combustibility limit; Porous media; Volatile organic compounds

1. Introduction

Ventilation gases purification from VOCs remains important problem for the painting, printing, chemical, pharmaceutical industries. There are many methods of flue gases purification: sorption, condensation, combustion (conventional or catalytic), membrane separation, chemical/biochemical transformation of pollutants to neutral or easily utilizable components [1–4]. Most of the methods are rather specific. The sorption process consumes sorbents. Condensation to liquid phase is appropriate for highly concentrated components characterized by relatively high temperature of condensation [1]. Membrane separation, catalytic oxidizing, chemical or biochemical transformation of the pollutants all remain expensive technologies, efficient only for specific cases [1,2]. VOCs thermal oxidation is probably the most universal method of pollution control. Direct combustion of the polluted air in the open flames is effective economically if the process is combined with industrial boiler, furnace or power generator. The last decade the regenerative thermal oxidation (RTO) technology utilizing VOCs oxidation in conditions of heat regeneration became widely spread. In spite of effective heat recirculation, powerful RTO systems consume considerable amount of fuel and are not ideal from this point of view. Combustion of extra-low calorific value VOCs polluted gases in superadiabatic conditions without consumption of fuel may be performed in non-steady filtration combustion waves.

Main principles of filtration combustion (FC) (or excess enthalpy combustion) were formulated by Weinberg [5], Fateev [6], Matros [7] and further developed in [8–12] and other works. The corner stone of the superadiabatic FC is interaction (coupling) of propagating thermal and combustion waves resulting in local superadiabatic temperature in the system. The relationship between maximum temperature T_{max}, FC wave propagation speed u_w and thermal wave speed u_{th} was determined theoretically and confirmed experimentally

* Corresponding author. Tel.: +375 17 284 2021; fax: +375 17 284 2212.
E-mail address: kdob@itmo.by (K.V. Dobrego).

0017-9310/$ - see front matter © 2007 Elsevier Ltd. All rights reserved.
doi:10.1016/j.ijheatmasstransfer.2007.11.017

Nomenclature

c	heat capacity (J/kg/K)
d_0	diameter of porous media particle (m)
d_p	diameter of porous media pore (m)
$\mathbf{D}$	gas diffusivity tensor (m^2/s)
$\mathbf{D}_d$	dispersion diffusivity tensor (m^2/s)
D_p, D_t	longitudinal and transverse component of dispersion diffusivity tensor
D_g	gas diffusivity coefficient (m^2/s)
E	chemical reaction activation energy
G	gas mixture specific mass flow rate
h_i	mass enthalpy of ith chemical component
Δh	gas mixture heat of combustion (J/kg)
$\mathbf{I}$	unit matrix
k_0, k_1	filtration permeabilities
L	length of system
l_0	mean photon free path
M	average molecular weight of gas (kg/mol)
m	porosity
Nu	Nusselt number
p	pressure (Pa)
p_0	outlet pressure (Pa)
Pr	Prandtl number
Q^+, Q^-	heat (enthalpy) source and sink
R	universal gas constant
Re	Reynolds number
S_{sp}	porous body specific area (m^2/m^3)
T_0	inlet gas or ambient temperature ($\Delta T = T - T_0$)
T_{ad}	adiabatic temperature of combustion
T_{out}	average temperature of the flue gas
$\mathbf{u}$	gas velocity vector (m/s)
u_g	superficial gas velocity (m/s)
u_{th}	thermal wave velocity
u_w	combustion front velocity (m/s)
w	heat release rate
Y_i	mass fraction of ith component

Greek symbols

α_{vol}	volumetric heat exchange coefficient ($W/m^3/K$)
β	volumetric heat loss coefficient
$\delta = \tau_{ch} u_g$	characteristic length of chemical reaction
ε	emissivity of the porous carcass
φ	fuel/air equivalence ratio
ρ	density (kg/m^3)
$\dot{\rho}_i$	mass generation rate of ith component due chemical reactions (kg/s)
$\mathbf{\Lambda}$	heat conductivity tensor (W/m/K)
λ	heat conductivity (W/m/K)
μ	gas viscosity coefficient (Pa s)
σ	Stefan–Boltzmann constant ($W/m^2/K^4$)
$\boldsymbol{\tau}$	unit vector with components τ_z (τ_r)
τ_{ctrl}	flow direction switch time
τ_{ch}	chemical reaction time

Subscripts

g	gas
i	ith component of gas
s	solid
ins	insulation, refractory layer
max	maximum value
min	minimum of function
LCL	low combustibility limit

$$\Delta T_{ad}/\Delta T_{max} = 1 - (u_w/u_{th}). \quad (1)$$

Equation shows that maximum temperature in co-flow propagating FC wave may considerably (many times) exceed adiabatic combustion temperature T_{ad} [9,12].

The critical issue for FC technology application for VOCs oxidation is the lean combustibility limit (LCL). The lower LCL is attainable at FC reactor – the wider range of applications is possible, less polluted gases can be treated and more effective economically the technology is. The typical content and calorific value of the industrial ventilation gases is presented in the Table 1.

Different schemes of reactors may be utilized for the steady-state (quasi-steady-state) superadiabatic combustion [16]. The reciprocal flow reactor (RFR) is one of the most effective. RFR reproduces superadiabatic FC wave periodically by switching flow direction, Fig. 1.

Hanamura with colleagues [13] investigated numerically a model RFR ($L = 1$ m, adiabatic) with sponge-type porous media. Constant heat and mass transfer coefficients and single step overall oxidation reaction were accepted for simulation. The LCL equivalent to mixture with calorific content 65 kJ/m^3 was obtained. It corresponds to adiabatic combustion temperature $\Delta T_{ad} \sim 50$ K. Several important parametric dependencies were investigated, particularly the influence of the flow direction switch time τ_{ctrl} on the maximum temperature and combustion efficiency; the flame extinguishing limits were recognized and

Table 1
The typical content and calorific value of the industrial ventilation gases

Technology	VOC components	Concentration	dT_{ad}/K
Painting shop	Xylol, toluene, acetone, butyl acetate, white-spirit, etc.	0.5 (g/m^3)	15
Polymer (plastics) extruder shop	Formaldehyde, phenol, acetic acid, styrene, acetaldehyde, etc.	500–1000 ppm	30–60

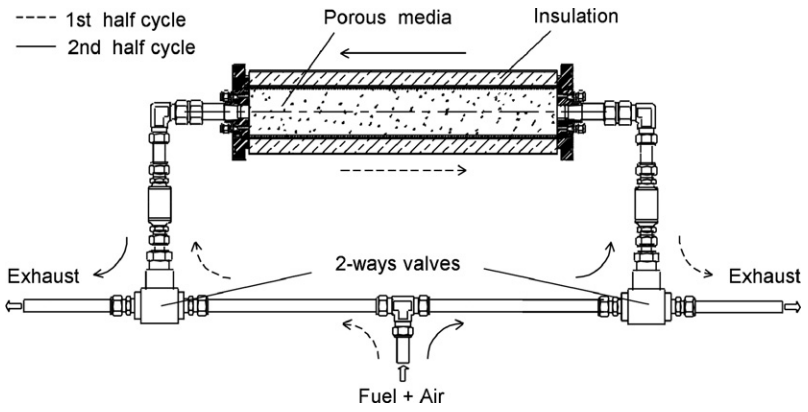

Fig. 1. Scheme of reciprocal flow filtration combustion reactor.

described by respect of thermal conductivity of the porous media, PM heat capacity, inter phase heat transfer coefficient and other parameters. To a pity investigations were not related to practical setup, undertook considerable model simplifications and did not reveal several principal dependencies such as the system heat loss and the system length influence on the performance.

In the commercial report [14] it was declared that stable combustion of paint box ventilation gas was achieved for the gas heat content equivalent to $\Delta T_{ad} \sim 30$ K. No up to date information from this company is currently available.

Hoffmann and colleagues [10] have performed an experimental investigation of ultra lean methane–air mixture combustion in a lab scale RFR. Sponge-type ceramics with different pores size and characteristic dimensions $10 \times 10 \times 20\ \mathrm{cm}^3$ was used in experiments. The concentration lean limits corresponding to periodic quasi-steady operation were obtained for ceramics with 6, 13 and 30 pores per inch. Best LCL value obtained was $\varphi = 0.028$ ($\Delta T_{ad} \sim 81$ K) and for slightly increased reactor $14 \times 14 \times 35\ \mathrm{cm}^3 - \varphi = 0.026$, ($\Delta T_{ad} \sim 73$ K). Authors suppose that lower LCL can be obtained at a bigger scale devices.

The question of minimal possible LCL for this kind of reactors is still open. To answer this question LCL investigation as function of the reactors major parameters such as length, diameter, porous media properties, etc. should be performed. The absence of reliable investigations in this area hinders practical design and application of the technology. It is worth mention that LCL determination in the field of multiple parameters demands large computational resources and was an impossible task for desktop computers 5–10 years ago. A question of LCL is also linked to the problems of the FC stability and 2D effects, although this complicated questions are out of sight of this paper.

In this paper we estimate numerically the LCL in the field of main parameters of the system (intensity of heat losses, reactor's length, pressure, packed bed particle size, porosity). Qualitative theoretical analysis of the problem is performed. Important qualitative characteristics of the system are revealed. Non-monotonous dependence of LCL on flow rate is demonstrated, so that specific flow rate providing minimum LCL may be determined for the system. The results may be utilized for practical RFR design and optimization.

1.1. Analysis of factors defining LCL

Experimental and numerical investigations of reciprocal flow reactors (RFR) show that time averaged temperature profile in the system acquire symmetrical triangular shape when approaching LCL [10]. It is typical that small difference between the FC wave and thermal wave velocities $u_{th} \approx u_w$ takes place which is equivalent to $\Delta T_{ad}/\Delta T_{max} \ll 1$ according to (1). These facts give ground to consider extra-low calorific FC wave as isolated (single), quasi-stationary, symmetrical thermal wave with a heat source located at its top, Fig. 2.

In 1D, one-temperature approximation [9] FC system is described by heat conductivity equation

$$[(c\rho)_g + (c\rho)_s]\frac{\partial T}{\partial t} + (c\rho)_g u_g \nabla T = \lambda \Delta T - \beta(T - T_0) + w, \quad (2)$$

here indexes "g" and "s" relates to the gas and solid phases, $\lambda = \lambda_g + \lambda_s$ – effective heat conductivity, β – heat loss coefficient, w – chemical heat release term. In the moving with u_{th} speed coordinates equation reads

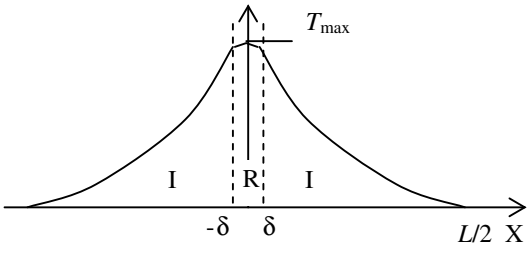

Fig. 2. Model quasi-steady temperature profile in reciprocal flow reactor. I – inert area, R – reacting area.

$$\frac{\partial T}{\partial x} = \Lambda\Delta T - B(T - T_0) + W.$$

Here $u_{\text{th}} = \frac{(c\rho)_g u_g}{(c\rho)_g + (c\rho)_s}$, $\Lambda = \frac{\lambda}{(c\rho)_g + (c\rho)_s}$, $B = \frac{\beta}{(c\rho)_g + (c\rho)_s}$, $W = \frac{w}{(c\rho)_g + (c\rho)_s}$.

Corresponding solution in the inert area ($w = 0$) is described by exponents

$$\begin{aligned} T &= T_0 + T_{\max}\exp\{-(x-\delta)\sqrt{\beta/\lambda}\}, \quad x > 0 \\ T &= T_0 + T_{\max}\exp\{(x-\delta)\sqrt{\beta/\lambda}\}, \quad x < 0 \end{aligned} \tag{3}$$

The reacting area may be considered as small "cap", Fig. 2. Experiment show that "cap" shrinks to its minimal width when the system approaches to LCL [10]. Minimum cap width δ is limited by combustion time τ_{ch} and gas-to-solid heat transfer distance $l_{g-s} \approx c\rho u_g/(\alpha\Delta T_{\text{ad}})$ (the length should be enough for complete combustion and gas-to-solid heat transfer) $-\delta \approx \tau_{\text{ch}} u_g + l_{g-s}$. The temperature corresponding to LCL may be estimated via non-liner analysis similar to the normal laminar flame flammability analysis [23], and roughly – from equation $\tau_{\text{ch}} u_g = L/2$. The $T_{\max}$ is weak function of the system parameters (as far as reaction time τ_{ch} is exponential function of temperature) and may be considered as constant here. Assuming $\delta \ll L$ and $T_{\max} = \text{const}$ one can estimate LCL by using energy balance, without resolution of the chemically reacting zone.

Stationary heat losses of the FC wave in the case of long (endless) system

$$\begin{aligned} Q^- &= \int \beta(T - T_0)\mathrm{d}x \\ &\cong 2\Delta T_{\max}\sqrt{(\lambda_g + \lambda_s)}\sqrt{\beta} + 2\delta\Delta T_{\max}\beta. \end{aligned} \tag{4}$$

Equating incoming enthalpy $Q^+ = (c\rho)_g u_g \Delta T_{\text{ad}}$ and heat loss, one can obtain

$$\frac{\Delta T_{\text{ad}}}{2\Delta T_{\max}} \cong \frac{\sqrt{\lambda}\sqrt{\beta}}{(c\rho)_g u_g} + \frac{\delta\beta}{(c\rho)_g u_g}. \tag{5}$$

Eq. (5) defines "permitted" quasi-steady regimes of RFR operation. LCL corresponds to minimum possible $\Delta T_{\max}$.

In the case of a short system, reactor's length L becomes important parameter. Integration of heat losses with respect to a boundary condition $T|_{x=L} = T_{\text{out}}$ and $\delta \ll L$ reads

$$\begin{aligned} T = T_{\text{out}} + \frac{T_{\max} - T_{\text{out}}}{1 - \exp\{-L/2\sqrt{\beta/\lambda}\}}\left(\exp\left(-x\sqrt{\beta/\lambda}\right)\right. \\ \left. - \exp\left(-\frac{L}{2}\sqrt{\beta/\lambda}\right)\right). \end{aligned} \tag{6}$$

The enthalpy delivered to the system is $Q^+ = (c\rho)_g u_g(\Delta T_{\text{ad}} - \Delta T_{\text{out}})$. As far as ΔT_{out} – is the third unknown parameter – it is impossible to express $\Delta T_{\text{ad}}/\Delta T_{\max}$ explicitly by using only energy balance equation. If $\Delta T_{\text{out}} \cong 0$ similar manipulations lead to expression

$$\frac{\Delta T_{\text{ad}}}{\Delta T_{\max}} \cong 2\frac{\sqrt{\lambda}\sqrt{\beta}}{(c\rho u)_g} - \frac{\beta L}{(c\rho u)_g}\frac{\exp\left(-L/2\sqrt{\beta/\lambda}\right)}{\left(1 - \exp\left(-L/2\sqrt{\beta/\lambda}\right)\right)}. \tag{7}$$

One – temperature approximation ($\alpha \to \infty$) appears to be too rough for further LCL analysis. In reality gas and solid temperature profiles are separated which results in additional heat losses (not complete heat transfer to solid body), Fig. 3.

The difference between gas and solid temperature may be estimated by

$$\begin{aligned} (c\rho u)_g \partial T/\partial x|_{x=L/2} &= \alpha_{\text{vol}}(T_{g,\text{out}} - T_{s,\text{out}}) \\ &\cong \alpha_{\text{vol}}(T_{g,\text{out}} - T_0), \end{aligned} \tag{8}$$

α_{vol}-volumetric heat exchange coefficient. Estimating $\partial T/\partial x|_{x=L/2}$ from (6) one can obtain

$$\Delta T_{g,\text{out}} = \Delta T_{\max}\frac{(c\rho u)_g}{\alpha_{\text{vol}}}\frac{\sqrt{\beta/\lambda}\exp(-L/2\sqrt{\beta/\lambda})}{1 - \exp(-L/2\sqrt{\beta/\lambda})}, \tag{9}$$

and

$$\begin{aligned} \frac{\Delta T_{\text{ad}}}{\Delta T_{\max}} \cong 2\frac{\sqrt{\lambda}\sqrt{\beta}}{(c\rho u)_g} - \frac{\beta L\exp(-L/2\sqrt{\beta/\lambda})}{(c\rho u)_g\left(1 - \exp(-L/2\sqrt{\beta/\lambda})\right)} \\ + \frac{(c\rho u)_g}{\alpha_{\text{vol}}}\frac{\sqrt{\beta/\lambda}\exp(-L/2\sqrt{\beta/\lambda})}{1 - \exp(-L/2\sqrt{\beta/\lambda})} \end{aligned} \tag{10}$$

Gas flow rate dependence comes into (10) directly and via expression for gas dispersion heat conductivity $\lambda \equiv \lambda_s + \lambda_g \cong \lambda_s + 0.5\, d_0(c\rho)_g u_g$. Characteristic dependencies built by (10) for typical values: $\lambda_s = 1$ W/(m K), $u_g = 1$ m/s, $(c\rho)_g = 1290$ J/(m^3 K), $d_0 = 6$ mm, $\beta = 56$ W/(m^3 K), $L = 0.5, 1, 2, 4$ m, $\Delta T_{\max} = 1000$ K, $\alpha_{\text{vol}} = 10^5$ W/(m^3 K) are plotted on the Fig. 4.

Analysis shows that PM heat conductivity reduction as well as reactor length growth has strong potential for

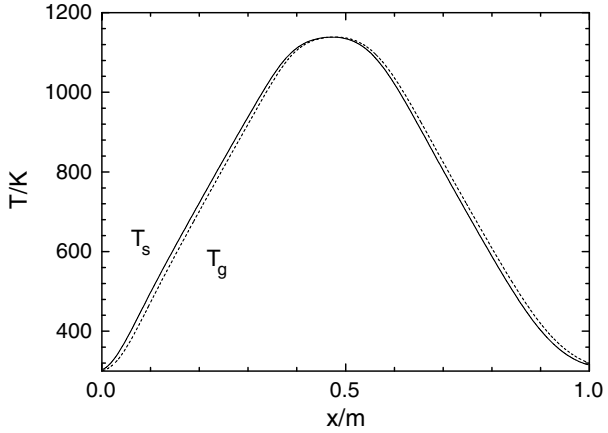

Fig. 3. Typical gas and solid phase temperature profiles. Numerical simulation for standard case (Table 2).

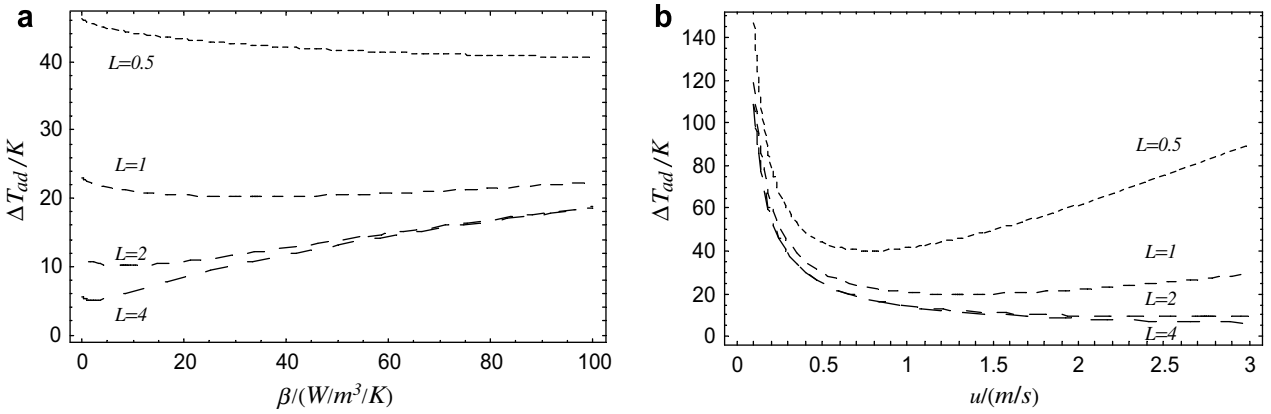

Fig. 4. Adiabatic temperature dependence on heat loss coefficient (a) and gas filtration velocity (b) at LCL. $L = 0.5, 1, 2, 4$ m as indicated on the graphs.

LCL improvement. Important result is non-monotonous behavior of the LCL curve as function of gas flow rate (Fig. 4b) and existence of optimum flow rate.

The above analysis was based on a numerous simplifications main of which are: small length of reacting zone, negligence of transient nature of the FC wave, assumption of thermal wave velocity $u_w \cong u_{th}$, T_{max} independence of flow rate and system parameters. Adequacy of the analysis should be verified by numerical simulations and experiments. Thus simulation show that non-monotonous behavior of the $\Delta T_{ad} = f(\beta)$ (Fig. 4a) is an artifact connected with mistakes in temperature profile solution (6). Simplest "triangular" temperature profile model applied to (8) gives $\Delta T_{g,out} = \Delta T_{max} \frac{(c\rho u)_g}{\alpha_{vol}(L/2)}$ and corresponding expression for $\Delta T_{ad}/\Delta T_{max}$ becomes free of the mentioned artifact.

1.2. Effect of pressure increase

The pressure may vary in the system due to variation of flow rate, ambient pressure or other technological reasons. Experimental and numerical investigations show that methane–air co-flow propagating FC waves slow down and the maximum temperature decreases with the pressure increase. The nature of this effect is elucidated by analytical formula for the temperature in filtration combustion wave [15]

$$T_{max} \approx E / \ln\left(\frac{Q\rho Y_{CH_4} z}{\alpha \Delta T_{ad}}\left(1 + \frac{\alpha\lambda}{G^2 c_g^2}\right)\right). \quad (11)$$

Density is proportional to pressure and other parameters do not depend on pressure in (11). Let's analyze the influence of pressure growth and corresponding temperature decrease on the chemical reaction length $\tau_{ch} u_g$ and heat transfer distance $l_{g-s} \approx c\rho u_g/(\alpha \Delta T_{ad})$. Taking into account that $T_{max} \sim E/\ln(c_1 p)$ (Eq. (11)), $\tau_{ch} \sim \exp(E/T)$ and $u_g \sim 1/p$, chemical reaction length as well as gas-to-solid heat transfer distance remain constants. Taking into account (9), (10), some LCL improvement will take place in the case of pressure increase.

2. Reciprocal flow reactor simulation

2.1. Basic equations

Conventional volume averaged two-temperature approximation was used for simulation of the system [15–18]. The set of equations included continuity and filtration equations for gas, mass conservation equation for chemical components, thermal conductivity equations for gas and solid phase and ideal gas state equation.

$$\frac{\partial \rho_g}{\partial t} + \nabla(\rho_g \mathbf{u}) = 0. \quad (12)$$

$$-\nabla p = \frac{\mu}{k_0}\mathbf{u} + \frac{\rho_g}{k_1}|\mathbf{u}|\mathbf{u}. \quad (13)$$

$$\rho_g \frac{\partial Y_i}{\partial t} + \rho_g \mathbf{u}\nabla Y_i - \nabla \rho_g \mathbf{D}\nabla Y_i = \dot{\rho}_i. \quad (14)$$

$$\rho_g c_p \frac{\partial T_g}{\partial t} + c_p \rho_g \mathbf{u}\nabla T_g - \nabla\Lambda\nabla T_g = \frac{\alpha_{vol}}{m}(T_s - T_g) - \sum_i h_i \dot{\rho}_i. \quad (15)$$

$$(1-m)\rho_s c_s \frac{\partial T_s}{\partial t} - \nabla(\lambda \nabla T_s) = \alpha_{vol}(T_g - T_s) - \beta(T_s - T_0) \quad (16)$$

$$\rho_g = \frac{pM}{RT_g}. \quad (17)$$

Gas diffusivity and conductivity terms in Eqs. (14) and (15) is a sum of gas molecular transport and dispersion terms $D = D_g + D_D$. The dispersion terms has the form [19] $D_D = 0.1\, d_0 u_g$ and $\Lambda_D \equiv \frac{\lambda_D}{(c\rho)_g} = D_D$. Thermal conductivity of porous media includes solid matrix conductivity λ_s and radiation conductivity components

$$\lambda = \lambda_s + (16/3)\varepsilon\sigma T^3 l_0, \quad (18)$$

where $\sigma = 5.67 \times 10^{-8}$ W/m^2/K^4 – Stefan–Boltzmann constant, ε – porous media surface emissivity, l_0 – mean photon free path. The volumetric convective heat transfer coefficient α_{vol} is used in the form suggested by [20]:

$$\alpha_{\mathrm{vol}} = S_{\mathrm{sp}} h,$$
$$S_{\mathrm{sp}} = 6(1-m)/d_0, \quad h = Nu\lambda_{\mathrm{g}}/d_0, \quad Nu = 2 + 1.1 Pr^{1.3} Re^{0.6}. \tag{19}$$

Molar heat capacity of k-th substance c_{p_k}, average molar heat capacity c_{p}, kth component molar enthalpy h_{k} and average enthalpy per one mole of mixture H are calculated by polynomial formulas in accordance with CHEMKIN procedures and database [21]. Other temperature dependent gas properties (μ, D_{g}, λ_{g}) were calculated by explicit approximate formulas, having characteristic accuracy 5% in all the temperature range. (Note that dispersion prevails over molecular transport in FC system which makes accuracy issues for D_{g}, λ_{g} calculation unimportant). Values of parameters of the system in the standard case are presented in the Table 2.

One step overall reaction $CH_4 + 2O_2 \rightarrow CO_2 + 2H_2O$ was considered for methane–air mixture FC. The first order by both CH_4 and O_2 and the reaction rate constant $k = 2.6 \times 10^8 \exp(-15640/T_{\mathrm{g}}) \frac{\mathrm{m}^3}{\mathrm{s\ mol}}$ was accepted.

2.2. Boundary conditions

The system (12)–(17) is added with boundary conditions for temperature, concentration and filtration velocity. Conditions of zero diffusion flows through chamber boundaries and internal walls $(\mathbf{n}\cdot\nabla) Y_i = 0$, as well as wall impermeability $(\mathbf{n}\cdot\nabla)p = 0$, are applied for the equation of mass conservation (14) and filtration (13), where $\mathbf{n}$ – normal to boundary unity vector. Gas temperature and concentrations are fixed at the entrance to the system and pressure – at the exit:

$$T_{\mathrm{g}}(z=0) = T_0; \left\{ Y_i(z=0) = Y_i^{\mathrm{entrance}} \right\}, \quad p(z=L) = p_0. \tag{20}$$

Table 2
Parameters of the RFR system for the standard case

Parameter	Dimension	Value	Description
L	m	2	Reactor (porous media) length
D_0	m	0.2	Reactor (porous media) diameter
d_0	m	6×10^{-3}	Packed bed particle diameter
β	W/m^3/K	50	Volumetric heat loss coefficient
p_0	Pa	1.013×10^5	Pressure at exit of reactor
ε	–	0.6	Emissivity of the PM particle surface
m	–	0.4	Porosity
ρ_{s}	kg/m^3	2810	PM particle material density
c_{s}	J/kg/K	794	PM particle material thermal capacity
λ_{s}	W/m/K	0.2	Thermal conduction coefficient of the porous media
D_{p}, D_τ	m^{-1}	0.5, 0.1	Dispersion coefficients
σ	–	Variable	Fuel – oxidizer equivalent ratio
G	kg/m^2/s	1	Gas mixture mass specific flow rate

Packed bed – Al_2O_3 balls.

The side losses of the system in 1D case are simulated by applying the proper value for the heat loss coefficient β in energy Eq. (15). This procedure is proved to be adequate for the case [8,16] when predominant part of the total temperature drop in the system ($T_{\max} - T_0$) comes to insulation layer and heat flux is in the steady-state (time averaged value of β). Then heat loss coefficient is expressed via insulation thermal conductivity λ_{isl}, radius of the reactor chamber R_0 and radius of the system including thermal insulation layer – R_2.

$$\beta = \frac{2\lambda_{\mathrm{isl}}}{R_0^2 \ln(R_2/R_0)}. \tag{21}$$

2.3. Numerical simulation method

Lean combustibility limit can be determined experimentally by gradual reduction of the equivalence ratio until steady-state becomes impossible.

The analogous procedure is realized numerically. Filtration combustion is initialized in reactor by heating up of its central part. The value of the system parameters in the standard case are presented in the Table 2. FC regime stabilization takes considerably much time. The criterion for the regime stabilization is 0.001% coincidence of the maximum temperature $T_{\max}$ and combustion (maximum heat release) coordinate from cycle to cycle. After the fact of regime stabilization methane concentration in the fuel mixture reduced by 5% and calculations continue. At certain moment the system cannot stabilize and temperature gradually reduces until chemical reaction stops. The system parameters encountered at the step prior to a system cool down correspond to LCL within ~5% accuracy by methane concentration (or equivalence ratio). The same procedure being repeated for different mixture flow rates defines LCL curve on the "methane–air equivalence ratio – Gas flow rate" ($\varphi - G$) plane. The array of the named curves obtained for different system parameters describes the system in view of lean combustion capabilities.

3. Model verification

Experiments by Hoffmann and colleagues [10] were simulated for the model verification. As far as foamed ceramics porous media was utilized in experiments, the correlations for PM heat conductivity, heat transfer and gaseous dispersion were corrected appropriately. Main parameters of the porous media were taken from the paper: porosity $m = 0.875$, pores size $d_{\mathrm{por}} = 2.56$ mm (corresponds to 13 pores per inch); PM surface emissivity $\varepsilon = 0.8$; volumetric heat loss coefficient $\beta = 80$ W/(m^3 K) (estimated by (17)); solid density $\rho = 3200$ kg/m^3, solid body conductivity $\lambda_{\mathrm{s}} = 1$ W/(m K), solid heat capacity was approximated by empirical equation [22] $c_{\mathrm{s}} = 197.79507 \cdot e^{\frac{197.79507}{T_{\mathrm{s}} - 49.25687}}$ J/kg K.

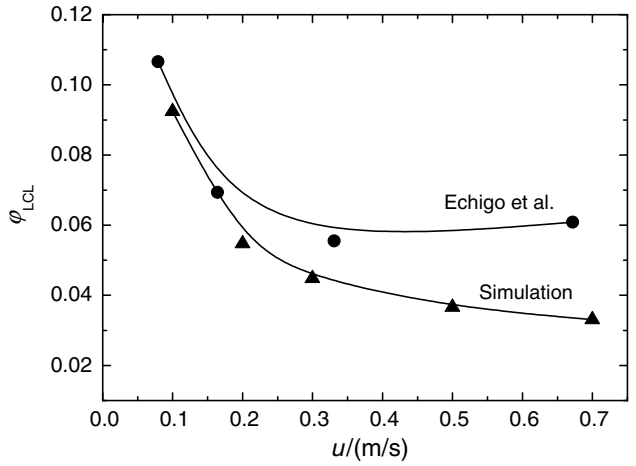

Fig. 5. Comparison of the experimental data [10] and numerical simulation of the LCL. 13 pores per inch SiC ceramics.

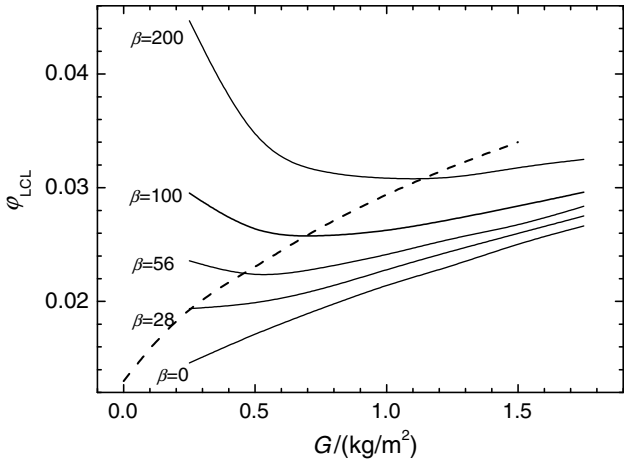

Fig. 6. Reciprocal flow reactor lean combustibility limit curves on the $\varphi - G$ plain. β values are on the graph. Dash line links minimum points of the LCL lines.

Volumetric heat transfer coefficient α was calculated according to (19) where solid particle diameter was estimated as $d_0 = \frac{2}{3}\frac{1-m}{m}d_{por}$ and specific area $S_{sp} = \frac{4m}{d_{por}}$. Then

$$\alpha_{vol} = \frac{6m^2\lambda_g}{d_{por}^2(1-m)}(2 + 1.1Re^{0.6}Pr^{1/3}) \quad (22)$$

The radiation conductivity coefficient is calculated according to (18) where photon free path was taken equal to pore size $l_0 = d_{por}$.

The gas fuel mixture utilized in experiments (methane, ethane and propane in the volumetric ratio 88: 5.8: 4.5: 1.7) was replaced with methane for the numerical experiments. Simulated and experimental LCL curves are presented in the Fig. 5.

One can observe reasonable quantitative and qualitative correspondence between the curves. Discrepancy is explained by multiple factors main of which is chemical kinetics model mistakes.

4. Results and discussion

Lean combustibility limit was evaluated at different values of the system parameters (heat loss coefficient β, reactor length L, packed bed particle diameter d_0, porosity m, pressure at the exit of reactor p_0). The standard reactor's LCL was defined first and then parameters were varied to obtain sets of LCL curves on the equivalence ratio – mass flow rate ($\varphi_{LCL} - G$) plane.

LCL curves obtained for different volumetric heat loss coefficients including adiabatic case ($\beta = 0$) are presented on the Fig. 6. Note that coefficients $\beta = 28, 56, 100, 200$ W/(m^3 K) correspond to insulation layer width $L_{ins} = 19, 7, 3.5$ and 1.6 cm ($\lambda_{ins} = 0.15$ W/(m K) and standard reactor dimensions). Simulation results indicate existence of minimum on the curves in accordance with the analytical results (Fig. 4). Adiabatic reactor LCL curve grows monotonously. Location of the minimums of the function $\varphi_{LCL,min}$ shifts to higher flow rate with β growth as indicated on the figure by dashed line. The fact of extremum existence at LCL curve has important practical implication defining the range of flow rates suitable for maximum performance of VOC oxidizers. The physical reason of extremum as follows from (10) is concurrence of two tendencies – improvement of energy balance (decrease of relative side heat loss) and relative decrease of heat exchange between gas and solid. To verify this conclusion additional LCL curve was determined for the standard system and in the case of radically increased heat exchange coefficient $\alpha_{vol} = 10^8$ W/(m^3 K), Fig. 7.

The question of the reactor length influence on the LCL is considered as rather simple one usually: the bigger length of the reactor the lower LCL is foreseen. Numerical investigation shows peculiarity of the system behavior. The LCL curves were determined for various lengths of reactors Fig. 8. Generally, as expected, longer reactors provide lower φ_{LCL}. At the same time the flow rate corresponding to a minimum φ_{LCL} grows. Simultaneous increase of the reactor's length and gas flow rate will result in rapid

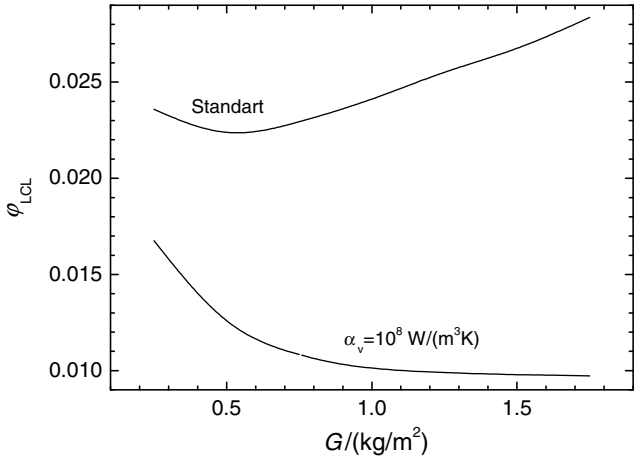

Fig. 7. LCL curves for standard case and case of radically increased volumetric heat exchange coefficient.

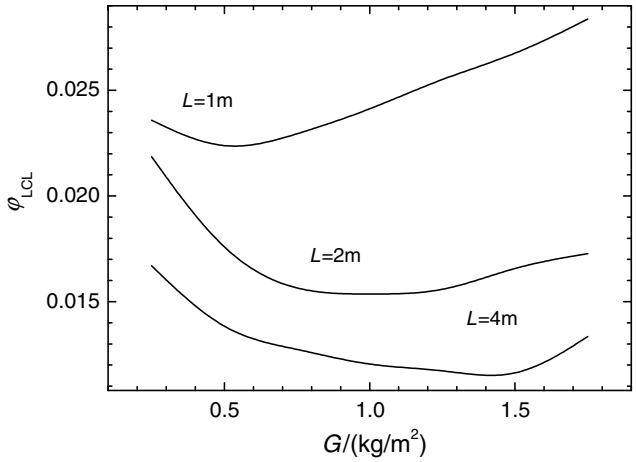

Fig. 8. Reciprocal flow reactor lean combustibility limit curves on the $\varphi - G$ plain. L values are on the graph.

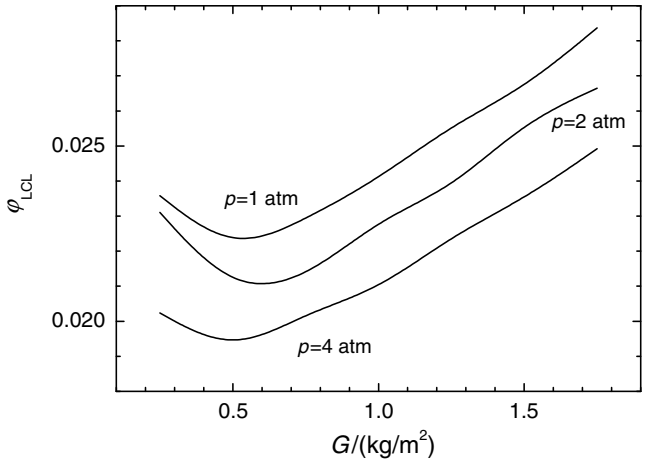

Fig. 10. Reciprocal flow reactor lean combustibility limit curves on the $\varphi - G$ plain. p_0 values are on the graph.

growth of the pressure drop and pumping cost. From the other hand longer reactors are usually characterized with bigger diameter and small β value.

The particle size has complex influence on the reactor performance, associated with dispersion conductivity, photon free path, specific area of porous media and other second order effects. The numerical simulation gives overall picture in this sense, Fig. 9. It is of particular importance the fact of decrease of the steepness of the LCL curves growth with flow rate and disappearance of extremum for the packed beds comprised of very small particles, Fig. 9. Note that monotonous behavior of the curves is preferable from the viewpoint of operation control.

The pressure in the system plays some noticeable role in the LCL control, Fig. 10. Numerical experiments show (in concord with analysis) that the LCL concentrations decrease at higher pressure, while corresponding curves remain quite similar, Fig. 10. The physical reason for that is the decrease of maximum temperature. Pressure variation may be utilized for the reactor operation control.

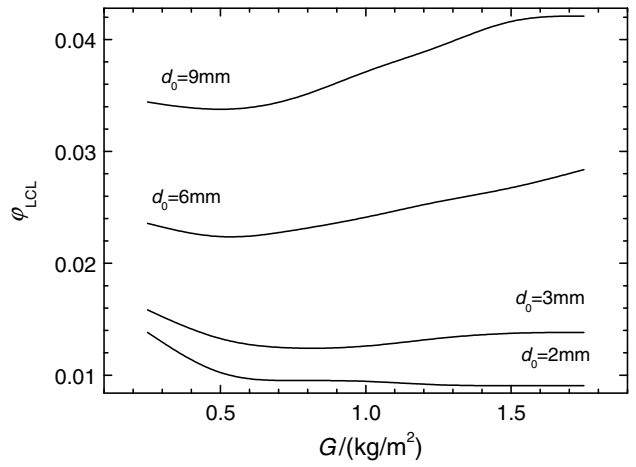

Fig. 9. Reciprocal flow reactor lean combustibility limit curves on the $\varphi - G$ plain. d_0 values are on the graph.

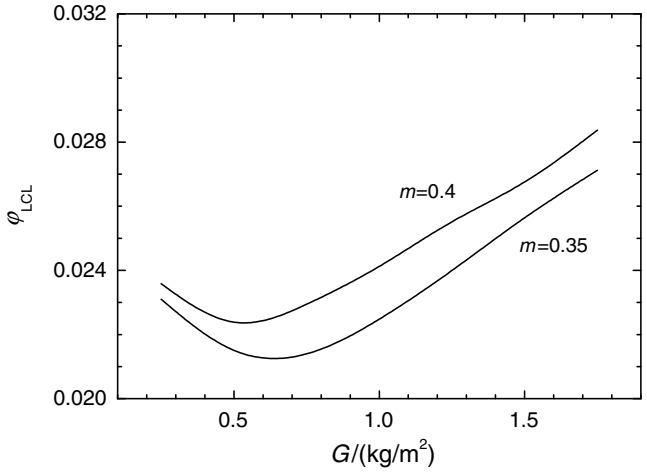

Fig. 11. Reciprocal flow reactor lean combustibility limit curves on the $\varphi - G$ plain. m values are on the graph.

Automatic valves may effectively increase the pressure and serve for combustion stabilization in appropriate cases. From the other hand pumping expenses considerably grow in the case of big pressure drop and big flow rate.

Numerical simulation demonstrates that small variation of porosity adequate to a packed bed of solid particles does not have considerable influence on LCL, Fig. 11. Transition to foamed ceramics can be effective solution for LCL reduction. From the other hand, the packed beds are more adequate to practical technological applications because of better thermo-mechanical stability and tolerance to thermo-cycling. Utilization of packed beds with increased porosity may be effective for pressure drop reduction.

5. Conclusions

Analytical and numerical investigation of methane–air lean combustibility limit in reciprocal flow filtration combustion reactor was performed. Investigation is particularly oriented on solution of the problem of reciprocal

flow reactors scale up, their adaptation for industrial utilization, determination of practically attainable lean combustibility limits and lean limit operation control.

Analytical expression for LCL is obtained. It is demonstrated that analytical correlation correspond qualitatively to detailed simulations and may be utilized for qualitative analysis of LCL for filtration combustion reciprocal flow reactors.

The method of numerical estimation of LCL reproduces conventional experimental procedure for LCL estimation. Numerical model and method was verified by using experimental data by Hofmann and Echigo [10]. Satisfactory accuracy of numerical procedure was proved.

The methane–air equivalence ratio corresponding to LCL was evaluated as a function of gas mass flow rate. Practically important parameters (heat loss coefficient, reactor length, pressure, particles size, porosity) were varied and corresponding sets of LCL curves were analyzed. The principal finding of the numerical investigation is existence of extremum – minimal possible LCL of function $\varphi_{\mathrm{LCL}} = f(G)$. The flow rate corresponding to the minimal LCL $G_{\mathrm{LCL,min}}$ grows together with heat loss coefficient (Fig. 6). It is shown that interphase heat exchange is responsible for the specific non-monotonous behavior of the function.

It is found that higher flow rate correspond to $G_{\mathrm{LCL,min}}$ for longer reactors. Thus to reach the minimal LCL for long reactor comparatively high flow rate is necessary, which will result in higher pressure drop and pumping energy losses. The advantage of long reactors becomes less at small flow rates.

Simulation shows that the porous media particle size is the most important factor influencing LCL, Fig. 8. Particle size decreasing not only shifts the LCL down, but changes the character of the function reducing steepness of the growing branch of the LCL line. For the particles smaller than 2 mm the LCL line goes down monotonously, as shown on Fig. 9.

The pressure in the system play considerably small role in the LCL control, Fig. 10. LCL curves remain similar at different pressures operation. The pressure variation may be utilized for the reactor operation control in appropriate cases.

Acknowledgement

This work was supported by Korean Federation of Sciences and Technology Societies (KOFST) Brain Pool Program.

References

[1] R.J. Martin et al., Selecting the most appropriate HAP emission control technology, Air Pollut. Consult. 3 (2) (1993) 1.1–1.9.

[2] K.B. Schnelle Jr., C.A. Brown in Air Pollution Control Technology Handbook, CRC Press, 2001, p. 408.

[3] B. Bretschneider, J. Kurfürst, Air Pollution Control Technology, Elsevier, 1987, p. 296.

[4] N.S. Torocheshnikov, A.I. Rodionov, N.V. Kelydev, V.N. Klushin, Technika zaschity okruzhaiuschei sredy, Chimia Publication, Moskow, 1981 (in Russian).

[5] F.J. Weinberg, Combustion temperature: The future? Nature 233 (1971) 239–241.

[6] G.A. Fateev, O.S. Rabinovich, Interaction of superadiabatic combustion and heat conversion waves in a porous medium with incorporated metal hydride elements, in: 27th Symposium (International) on combustion. The Combustion institute, Pittsburgg, PA, 1998, pp. 2451–2458.

[7] Yu.S. Matros, A.S. Noskov, V.A. Chumachenko, Catalytic Recreation of Industrial Flue Gases (in Russian), Nauka Publication, Novosibirsk, 1991, pp. 22–37.

[8] F. Contarin, A.V. Saveliev, A.A. Fridman, L.A. Kennedy, Int. J. Heat Mass Transfer 46 (2003) 949–961.

[9] L.A. Kennedy, A.A. Fridman, A.V. Saveliev, Superadiabatic combustion in porous media: wave propagation, instabilities, new type of chemical reactor, Int. J. Fluid Mech. Res. 22 (1995) 1–26.

[10] J.G. Hoffman, R. Echigo, H. Yoshida, S. Tada, Experimental study on combustion in a porous media with a reciprocating flow system, Combust. Flame 111 (1997) 32–46.

[11] W.D. Binder, R.J. Martin, The destruction of air toxic emissions by flameless thermal oxidation, Presented at 1993 Incineration Conference, Knoxville, Tennessee, 4 May, 1993.

[12] T. Takeno, K. Sato, An analytical study on excess enthalpy flames, Combust. Sci. Technol. 20 (1979) 73.

[13] K. Hanamura, R. Echigo, S. Zhdanok, Superadiabatic combustion in porous media, Int. J. Heat Mass Transfer 36 (13) (1993) 3201–3209.

[14] A new method of destroying organic pollutants in exhaust air. ADTEC Co., Ltd., Sweden, 1990. http://www.allbusiness.com/wholesale-trade/merchant-wholesalers-nondurable/445193-5.html.

[15] K.V. Dobrego, S.A. Zhdanok, Physics of filtration combustion of gases (in Russian), HMTI Publishers, Minsk, 2002.

[16] K.V. Dobrego, N.N. Gnesdilov, I.M. Kozlov, V.I. Bubnovich, H.A. Gonzalez, Numerical investigation of the new regenerator-recuperator scheme of VOC oxidizer, Int. J. Heat Mass Transfer 48 (2005) 4695–4703.

[17] K.V. Dobrego, I.M. Kozlov, S.A. Zhdanok, N.N. Gnesdilov, Modeling of diffusion filtration combustion radiative burner, Int. J. Heat Mass Transfer 44 (2001) 3265–3272.

[18] K.V. Dobrego, I.M. Kozlov, N.N. Gnesdilov, V.V. Vasiliev, 2D Burner – software package for gas filtration combustion systems simulation and gas non-steady flames simulation, Heat and Mass Transfer Institute, Minsk 2004 (Preprint N1).

[19] N. Wakao, S. Kaguei, Heat and Mass Transfer in a Packed Beds, Gordon and Breach, New York, 1982.

[20] M. Kaviani, Principles of Heat Transfer in Porous Media, Springer-Verlag, New York, Berlin, Heidelberg, 1995.

[21] R.J. Kee, F.M. Rupley, J.A. Miller, CHEMKIN-II: A fortran chemical kinetics package for the analysis of gas phase chemical kinetics, Sandia National Laboratory, SAND89-8009B, 1989.

[22] M.W. Chase Jr., NIST–JANAF themochemical tables (fourth ed.), J. Phys. Chem. Ref. Data Monogr. 9 (1998) 1–1951.

[23] Y.B. Zeldovich, G.I. Barenblatt, V.G. Librovich, G.I. Makhviladze, Mathematical theory of combustion and explosion, Consultants Bureau, New York, 1985.